Supplement of Atmos. Chem. Phys., 20, 10379–10400, 2020
https://doi.org/10.5194/acp-20-10379-2020-supplement

Atmospheric Chemistry and Physics
Open Access
EGU

Supplement of

Characterizing sources of high surface ozone events in the southwestern US with intensive field measurements and two global models

Li Zhang et al.

Correspondence to: Li Zhang (alex.zhang@noaa.gov)

This document contains Figures S1 to S14 and Table S1 to S6 not included in the main article.

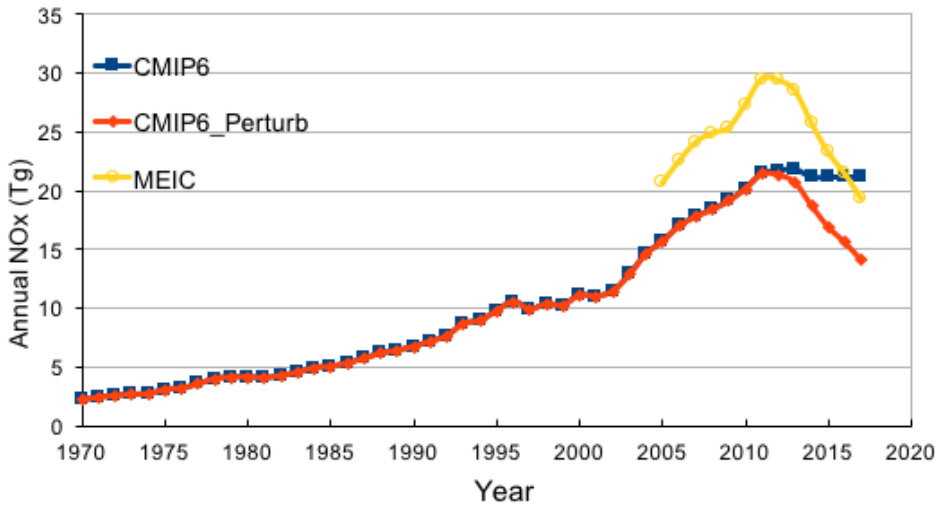

Figure S1. NO_X emission trends over China as estimated in the CMIP6 inventory (blue) and in MEIC (Multi-resolution Emission Inventory for China, yellow). The red line shows adjusted NO_X emissions used in this study.

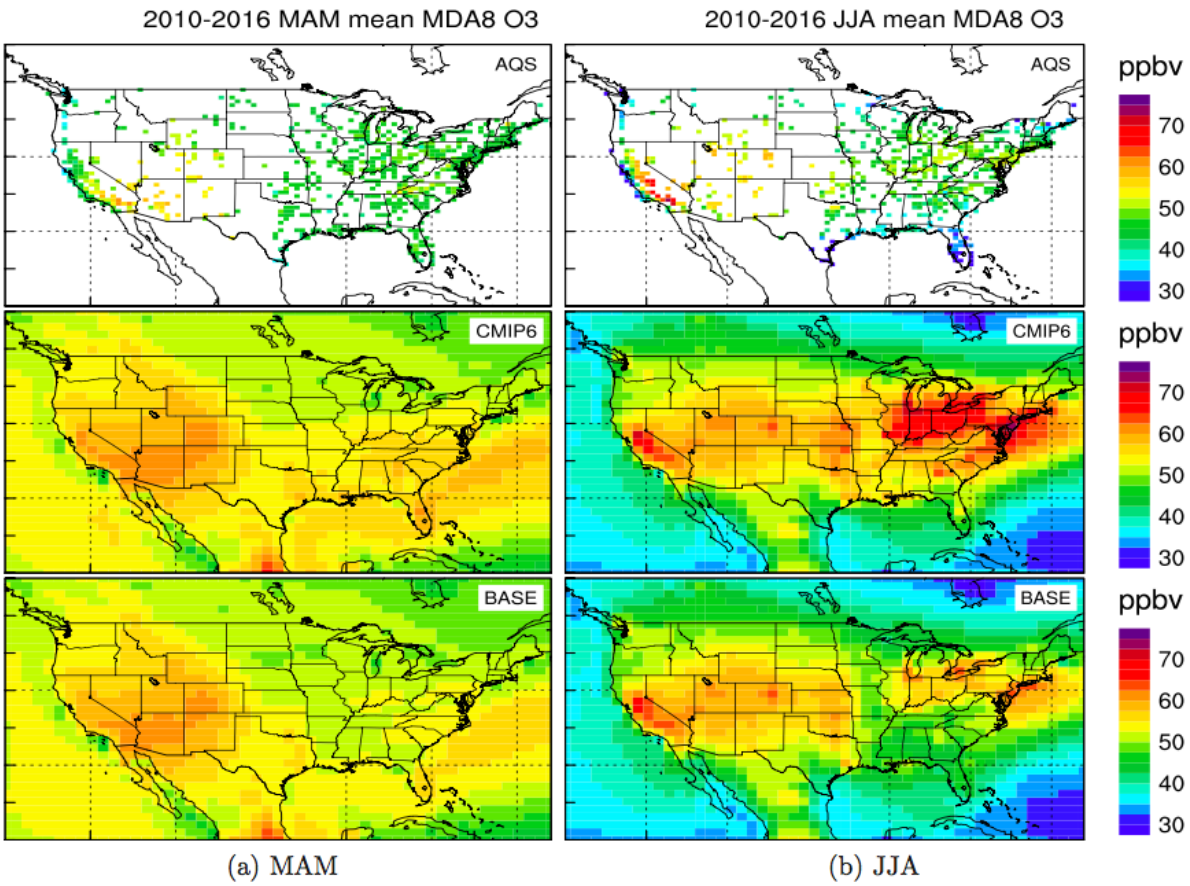

Figure S2. Spring (MAM) and summertime (JJA) mean MDA8 O_3 over the continental U.S. during 2010-2016 from AQS observations (top panels), GFDL-AM4 simulations with original CMIP6 emissions (middle panels) and adjusted emissions over the U.S. and China as described in the text (bottom panels) Observations at AQS sites are gridded into 0.5° × 0.625°.

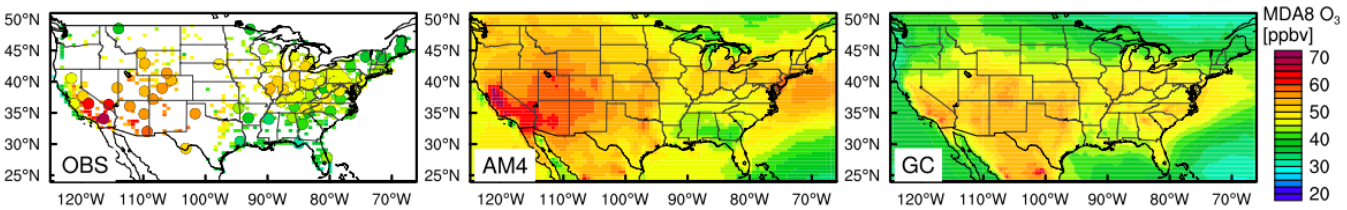

Figure S3. Spatial distributions of mean MDA8 O_3 during FAST-LVOS (May-June, 2017) as observed (OBS) and simulated with GFDL-AM4 (AM4) and GEOS-Chem (GC).

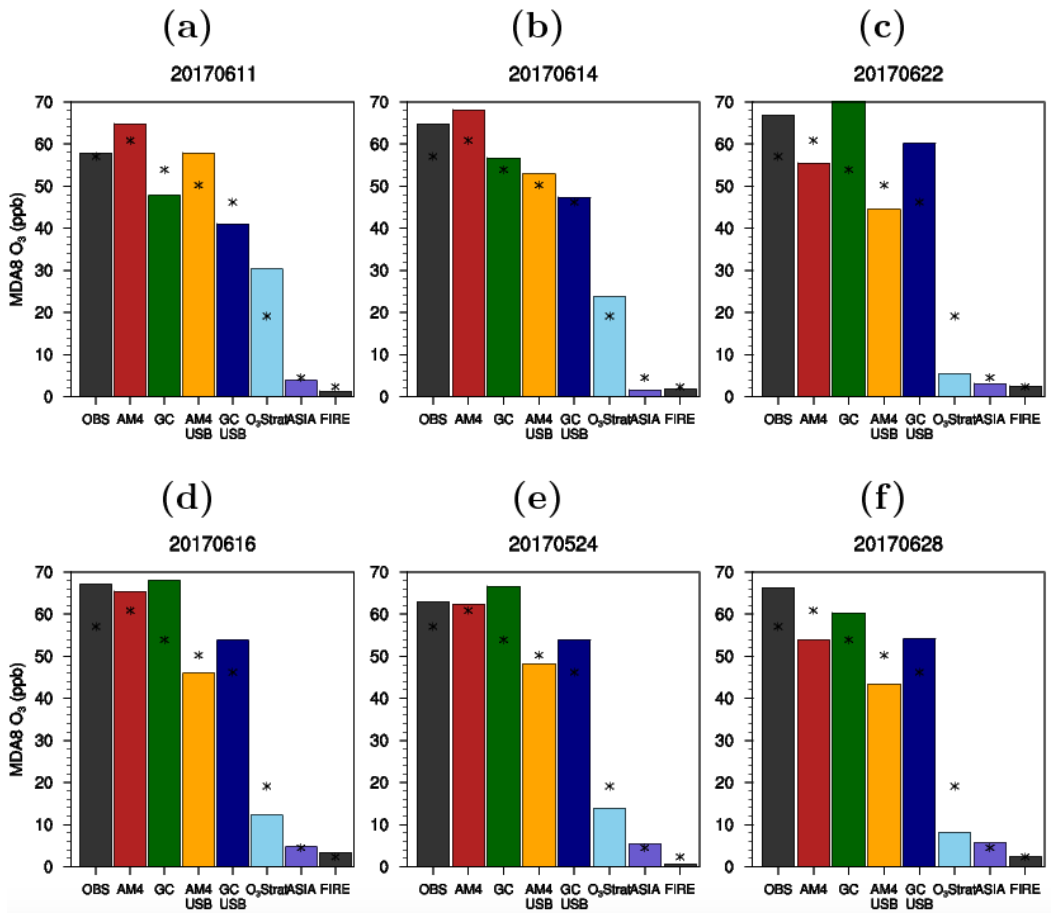

Figure S4. Statistics of MDA8 O_3 at 12 low-elevation (<1000 m altitude) air quality monitoring sites in the Las Vegas Valley as observed (OBS) and simulated with GFDL-AM4 (AM4) and GEOS-Chem (GC), along with USB O_3 from the two models, and contributions from stratospheric O_3 (O_3Strat), Asian pollution (ASIA), and wildfires (FIRE) estimated with GFDL-AM4 on (a) June 11, (b) June 14, (c) June 22, (d) June 16, (e) May 24, and (f) June 28, 2017. The star markers denote the mean values during the entire FAST-LVOS period (May-June, 2017).

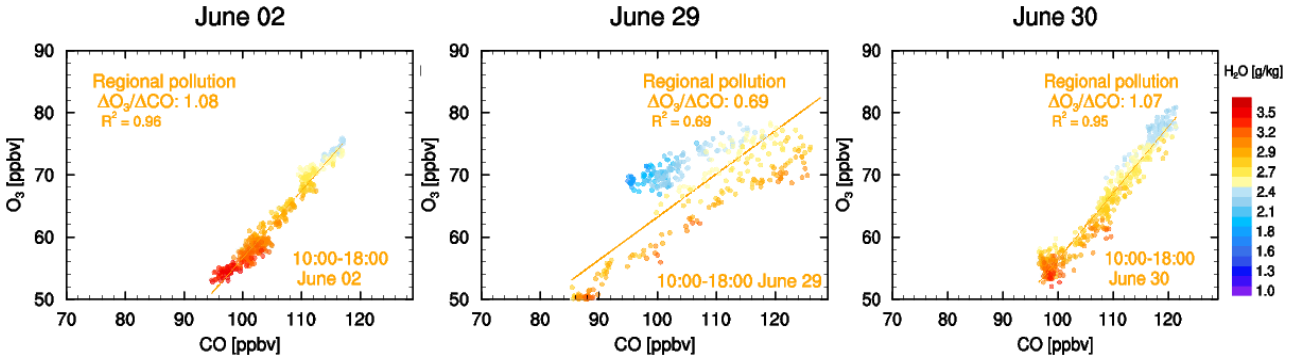

Figure S5. Scatter plots of 1-min O_3 against CO measured at Angel Peak, color-coded by specific humidity, for air masses influenced by regional pollution on June 02, June 29, and June 30.

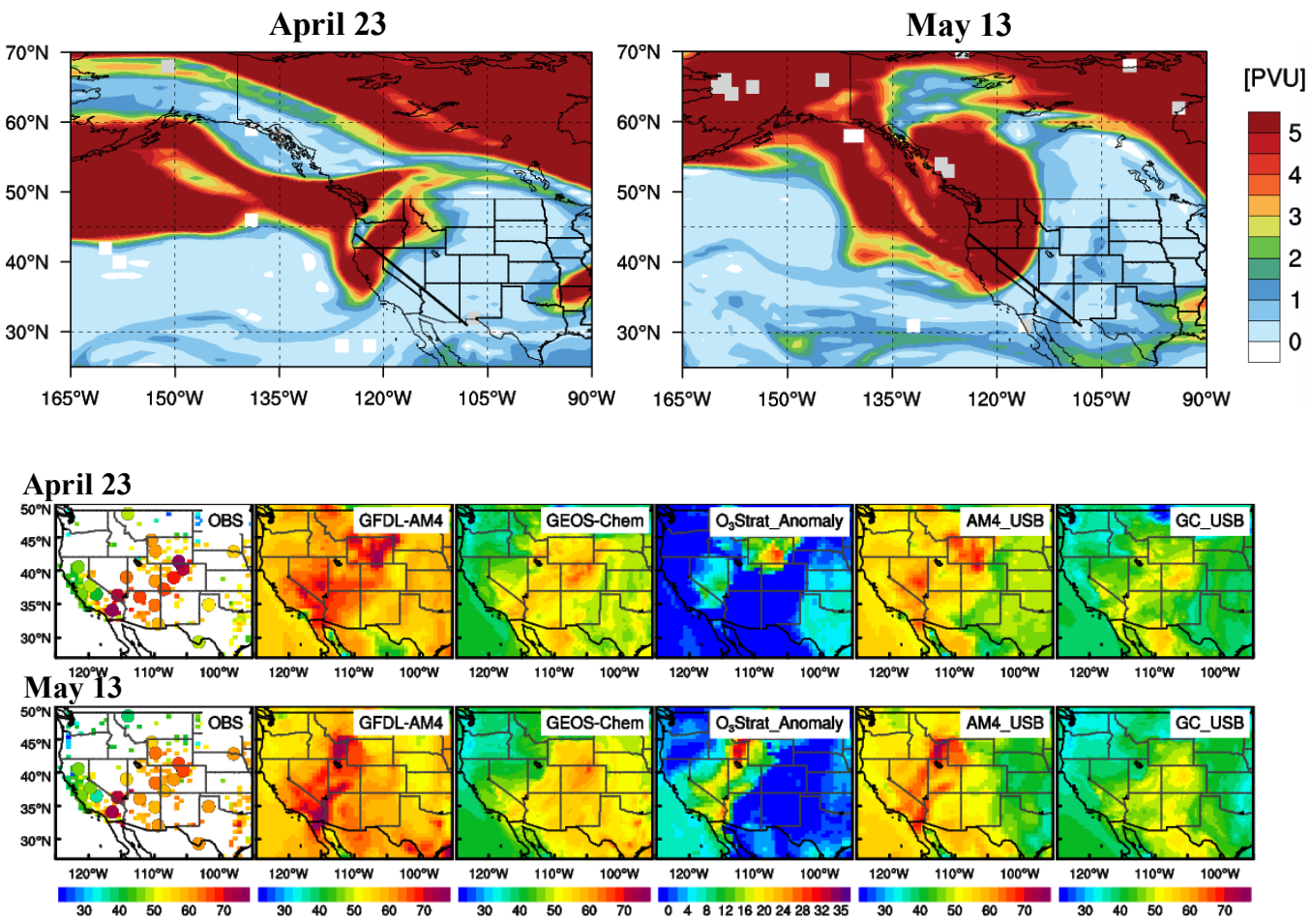

Figure S6. Top panels: Potential Vorticity at 250 hPa on April 23 and May 13 of 2017, calculated from the NCEP-FNL reanalysis data. Middle and bottom panels: maps of total MDA8 O_3 in surface air as observed and simulated with GFDL-AM4 and GEOS-Chem, along with anomalies of stratospheric O_3 tracer (relative to monthly mean) in AM4 and USB O_3 from the two models, during the STT events on April 23 and May 13 of 2017. Note that O_3Strat in this figure and Fig.9 is shown as anomalies relative to the monthly mean, while the absolute values are shown in Figs.4 and 8.

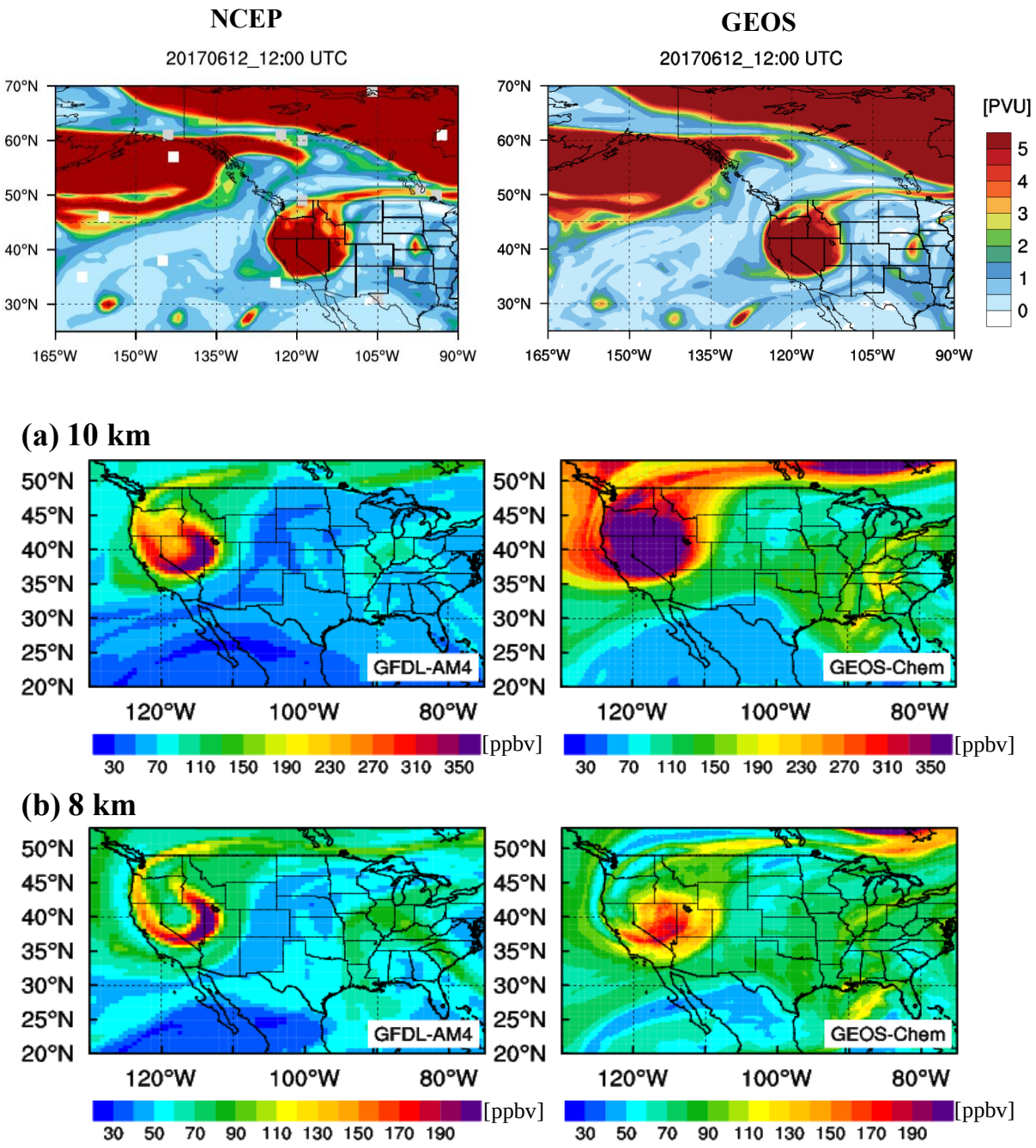

Figure S7. Top: Potential vorticity at 250 hPa on June 12 calculated from the reanalysis datasets used in AM4 (NCEP) and GEOS-Chem (GEOS). Bottom: Maps of O_3 levels at 10 km and 8 km altitude in GFDL-AM4 and GEOS-Chem on June 12, 2017.

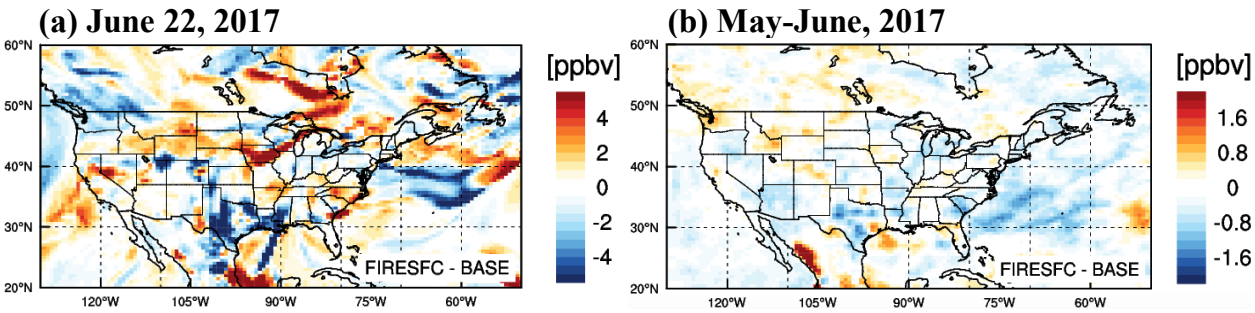

Figure S8. Differences in MDA8 O_3 between GFDL-AM4 FIRESFC (with all wildfire emissions placed at the surface) and BASE (a) on June 22, 2017 (wildfire event) and (b) during May-June, 2017 (FASTLVOS). Simulations are at C192 (~50 km × 50 km) horizontal resolution.

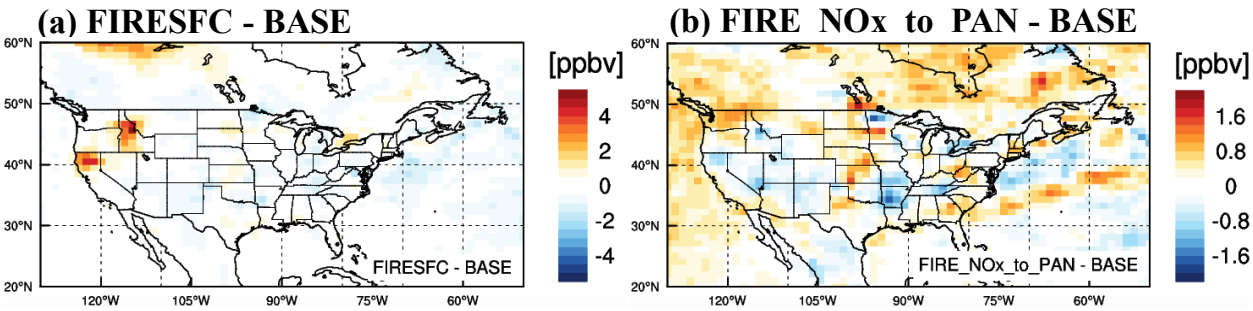

Figure S9. Monthly MDA8 O_3 differences during August, 2012 (an active wildfire season) between (a) GFDL-AM4 FIRESFC (with all wildfire emissions placed at the surface) and BASE and (b) difference between FIRE_NOx_to_PAN (with 40% and 20% of wildfire NOx partitioned into PAN and HNO_3, respectively) and BASE case. Simulations are at C96 (~100 km × 100 km) horizontal resolution. FIRE_NOx_to_PAN simulations are only available during 2010-2016.

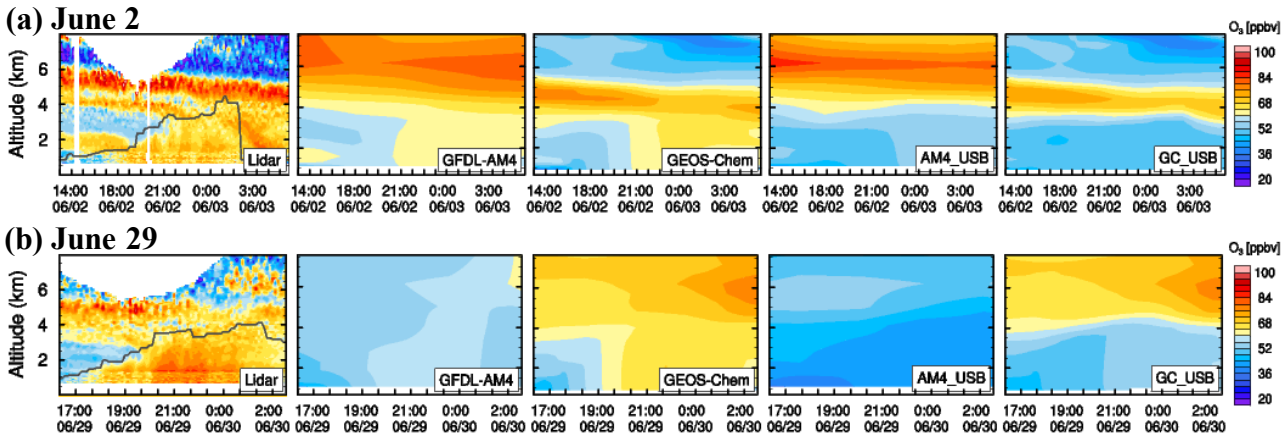

Figure S10. Time-height curtain plots of O_3 above NLVA as observed with TOPAZ lidar and simulated with GFDL-AM4 (~50×50 km^2; interpolated from 3-hourly data) and GEOS-Chem (0.25°×0.3125°; interpolated from hourly data) during the regional pollution events on (a) June 2 and (b) June 29, 2017 (UTC). The right panels compare USB O_3 from the two models.

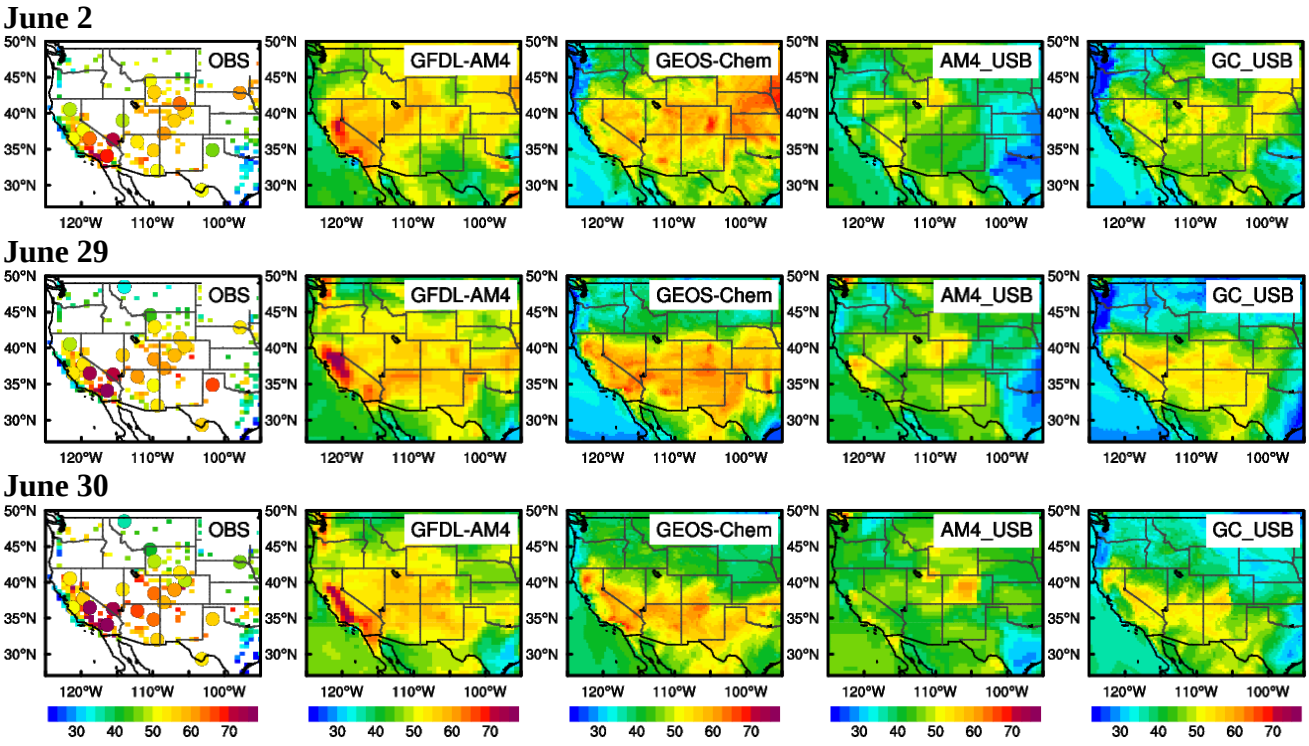

Figure S11. Maps of total MDA8 O_3 in surface air as observed and simulated with GFDL-AM4 and GEOS-Chem, along with USB O_3 from the two models, on June 2, June 29, and June 30.

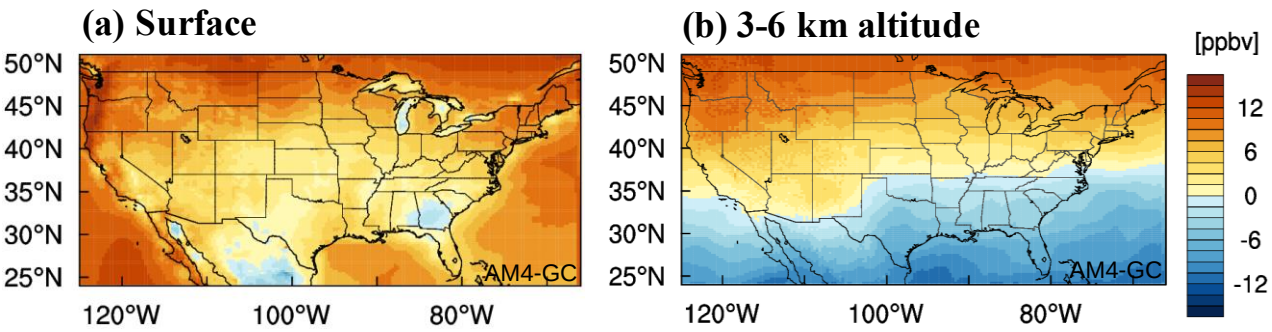

Fig. S12. Differences in USB O_3 between GFDL-AM4 and GEOS-Chem (a) at the surface (MDA8) and (b) between 3-6 km altitude (24-hour mean) during April-June, 2017.

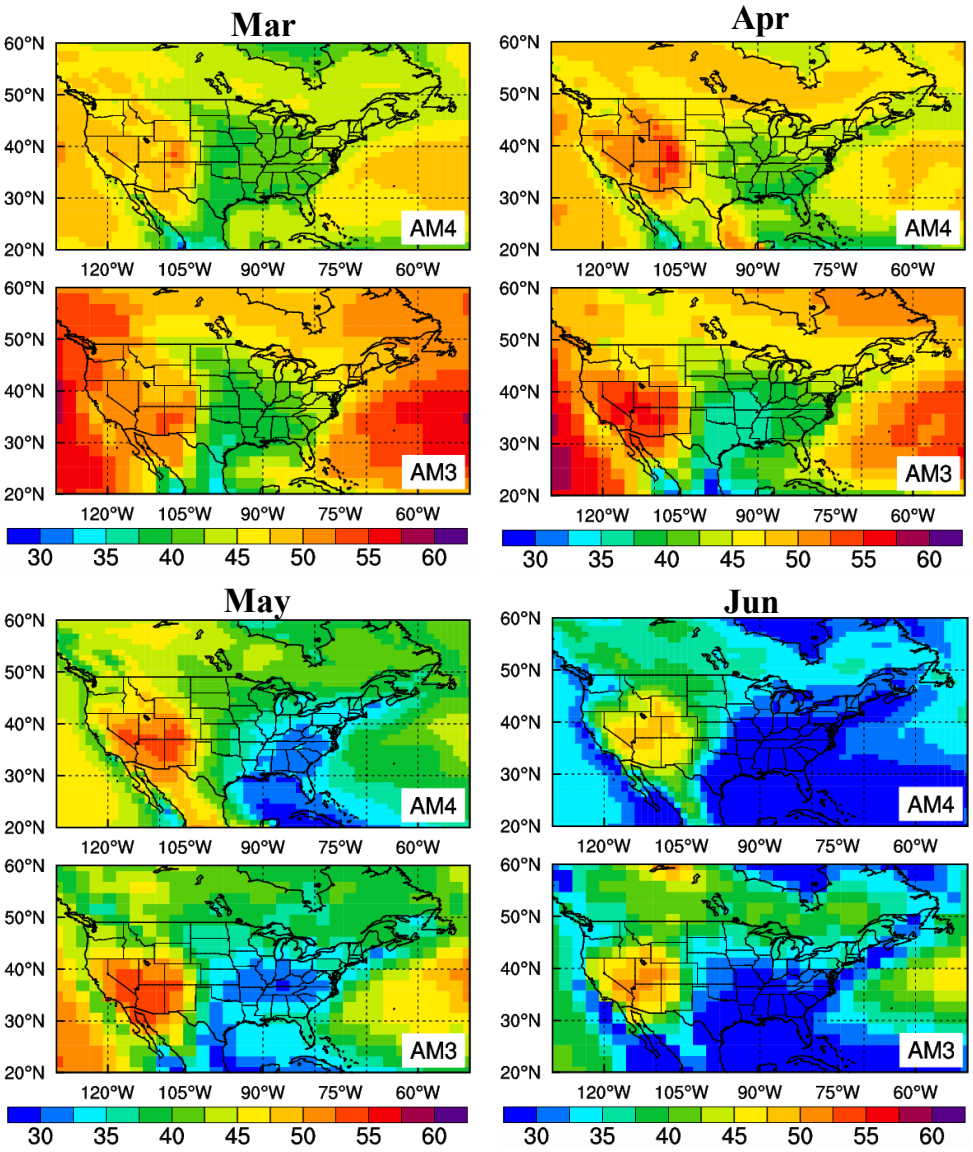

Figure S13. Comparison of surface NAB MDA8 O_3 estimates in the GFDL-AM4 model (this study) with its predecessor GFDL-AM3 (Lin et al., 2012a; Lin et al., 2017). The results are shown separately for March to June during the 2010-2014 period for which the NAB simulations are available from both models.

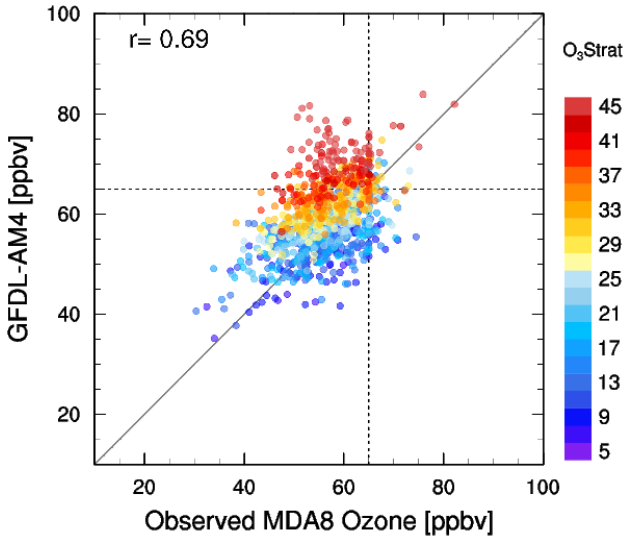

Figure S14. Scatter plots of observed versus simulated daily MDA8 O_3, color-coded by AM4 stratospheric O_3 tracer (O_3Strat) at 12 WUS high-elevation sites during April-June, 2017.

Table S1. Air quality monitoring sites in Clark County, NV and CASTNet sites in the western U.S. used in this study and statistics of model performance for MDA8 O_3 at these sites during April-June, 2017.

Site ID	Site Name	Latitude (º)	Longitude (º)	Elevation (m)	r (AM4/GC)*	MB (AM4/GC)*	NMB (AM4/GC)*	City/State
Clark County sites								
32-003-0601	Boulder City	35.98	-114.85	750	0.57/0.87	5.4/-3.3	9.8%/-6.1%	Boulder City, NV
32-003-0298	Green Valley	36.05	-115.05	562	0.60/0.86	5.0/-3.7	9.0%/-6.6%	Henderson, NV
32-003-1019	Jean	35.79	-115.36	924	0.51/0.81	5.5/-2.9	9.8%/-5.2%	Jean, NV
32-003-0043	Paul Meyer	36.11	-115.25	736	0.65/0.79	3.1/-5.9	5.4%/-10.1%	Las Vegas, NV
32-003-0071	Walter Johnson	36.17	-115.26	780	0.60/0.84	1.8/-7.2	3.0%/-12.1%	Las Vegas, NV
32-003-0073	Palo Verde	36.17	-115.33	939	0.59/0.84	3.0/-5.9	5.2%/-10.2%	Las Vegas, NV
32-003-0075	Joe Neal	36.27	-115.24	732	0.59/0.85	2.5/-6.5	4.3%/-11.1%	Las Vegas, NV
32-003-0540	Jerome Mack	36.14	-115.08	549	0.59/0.83	8.9/-0.2	17.1%/-0.4%	Las Vegas, NV
32-003-0022	Apex	36.39	-114.91	661	0.58/0.88	5.2/-3.7	9.4%/-6.6%	Apex, NV
32-003-0023	Mesquite	36.81	-114.06	488	0.62/0.79	8.5/-0.7	16.4%/-1.4%	Mesquite, NV
32-003-2002	JD Smith	36.19	-115.12	569	0.59/0.81	5.2/-3.8	9.4%/-6.7%	North Las Vegas, NV
32-003-7772	Indian Springs	36.57	-115.68	977	0.71/0.74	5.1/-3.0	9.2%/-5.4%	Indian Springs, NV
32-003-0078	Arden Peak	35.95	-115.04	1311	0.34/0.82	-0.4/-5.6	-0.7%/-9.2%	Henderson, NV
32-003-7771	SM Youth Camp	36.32	-115.59	2569	0.62/0.64	2.4/-5.5	4.1%/-9.5%	Las Vegas, NV
High-elevation sites (>1500 m above sea level)								
AP	Angel Peak+	36.32	-115.57	2682	0.50/0.72	-0.8/-4.6	-1.3%/-7.5%	Las Vegas, NV
CHA467	Chiricahua NM	32.01	-109.39	1570	0.59/0.77	2.1/-5.2	3.7%/-8.9%	AZ
PET427	Petrified Forest	34.82	-109.89	1723	0.52/0.78	3.3/-4.0	5.7%/-6.9%	AZ
GRC474	Grand Canyon NP	36.06	-112.18	2073	0.57/0.73	3.8/-5.4	6.7%/-9.5%	AZ
ROM406	Rocky Mountain NP	40.28	-105.55	2743	0.75/0.77	3.8/-2.0	6.8%/-3.6%	CO
GTH161	Gothic	38.96	-106.99	2926	0.82/0.69	3.1/-2.3	5.6%/-4.0%	CO
MEV405	Mesa Verde NP	37.2	-108.49	2165	0.65/0.76	3.9/-3.8	6.9%/-6.8%	CO
GRB411	Great Basin NP	39.01	-114.22	2060	0.75/0.80	6.0/-5.0	11.2%/-9.4%	NV
CAN407	Canyonlands NP	38.46	-109.82	1809	0.61/0.74	4.5/-5.1	8.0%/-9.2%	UT
PND165	Pinedale	42.93	-109.79	2388	0.79/0.79	4.4/-5.4	8.1%/-9.9%	WY
CNT169	Centennial	41.36	-106.24	3178	0.80/0.74	-0.2/-6.6	-0.3%/-11.4%	WY
YEL408	Yellowstone NP	44.56	-110.4	2400	0.75/0.82	5.7/-4.7	10.9%/-8.9%	WY

* r: day-to-day correlation coefficient between simulations and observations; MB: model mean bias; NMB: model normalized mean bias

+ NOAA mobile laboratory measurements

Table S2. Model configurations for GFDL-AM4 and GEOS-Chem BASE simulations.

Model	**GFDL-AM4**			**GEOS-Chem**		
Horizontal resolution	C96 (~100 km ×100 km) and C192 (~50 km×50 km) (Global)			2°×2.5° (Global) and 0.25°×0.3125° (North America)		
Vertical resolution	49 layers			47 layers		
Meteorological fields	Chemistry-Climate model; horizontal winds (u, v) are nudged to NCEP			GEOS-FP		
Tropospheric chemistry	Based on MOZART-2 (Horowitz et al., 2003; Horowitz et al., 2007)			Tropchem		
Stratospheric chemistry	Interactive (Austin and Wilson, 2006; Austin et al., 2013; Lin et al., 2015)			Linoz		
Biogenic isoprene	MEGAN2.1 (online)			MEGAN2.1 (online)		
Lightning NOx	Tied to model meteorological fields (Price and Rind, 1992) as described in Donner et al. (2011) and Naik et al. (2013)			Parameterized based on monthly climatology of satellite lightning observations coupled to model deep convection with a yield of 500 mol N/flash at northern mid-latitudes and 125 mol N/flash elsewhere (Murray et al., 2012)		
Anthropogenic emissions [a]	NOx (Tg N/yr)	CO (Tg/yr)	NMVOC (Tg/yr)	NOx (Tg N/yr)	CO (Tg/yr)	NMVOC (Tg/yr)
Western U.S.[b]	1.3	17.8	4.4	2.0	21.0	4.3
Eastern U.S.[c]	1.0	24.1	6.6	1.5	28.5	6.4
China	6.6	185.2	29.4	8.8	170.9	28.7
European Union	2.6	22.3	6.2	3.5	17.9	8.5
Wildfire emissions (Apr-Jun) [a]	NOx (Tg N)	CO (Tg)	NMVOC (Tg)	NOx (Tg N)	CO (Tg)	NMVOC (Tg)
Western U.S.[b]	0.013	0.615	0.113	0.013	0.615	0.122
Eastern U.S.[c]	0.010	0.614	0.125	0.010	0.614	0.135
China[d]	0.068	3.400	0.652	0.068	3.400	0.704
European Union	0.012	0.606	0.116	0.012	0.606	0.124

[a]See section 2.3 in the main article for the details of anthropogenic and fire emissions datasets used in this study.

[b] Western U.S.: 125-94.5◦W;

[c] Eastern U.S.: 94.5-60◦W;

Table S3. List of GFDL-AM4 and GEOS-Chem model simulations

Case	Simulation period	Emissions
GFDL-AM4		
C96_BASE	Jan 2010- Jun 2017	All anthropogenic emissions turned on (Section 2.3); daily fire emissions from FINN
C96_USB	Jan 2010- Jun 2017	Same as BASE with U.S. anthropogenic emissions turned off
C96_zeroAsia	Jan 2010- Jun 2017	Same as BASE with Asian anthropogenic emissions turned off
C96_zeroFire	Jan 2010- Jun 2017	Fire emissions turned off
C192_BASE	Jan- Jun 2017	Same as C96_BASE
C192_USB	Jan- Jun 2017	Same as C96_USB
C192_zeroAsia	Jan- Jun 2017	Same as C96_zeroAsia
C192_zeroFire	Jan- Jun 2017	Same as C96_zeroFire
GEOS-Chem		
GC_Global	Jan-Jun 2017	All anthropogenic emissions turned on (Section 2.3); daily fire emissions from FINN
GC_Global_USB	Jan-Jun 2017	Same as GC_Global, but with U.S. anthropogenic emissions turned off
GC_NA	Feb-Jun 2017	Nested simulations over North America with initial and boundary conditions from GC_Global
GC_NA_USB	Feb-Jun 2017	Nested simulations over North America with initial and boundary conditions from GC_Global_USB

Table S4. Statistics of model performance for MDA8 O3 in GFDL-AM4 (AM4) and GEOS-Chem (GC) at Clark County (CC) air quality monitoring sites and western U.S. CASTNet (CN) sites during each high-O3 episode analyzed in this study (locations of the sites are shown in Fig. 1). MB represents model mean bias and R denotes spatial correlation coefficient between simulations and observations.

Events	OBS (CC/CN)	AM4 (CC/CN)	GC (CC/CN)	MB_AM4 (CC/CN)	MB_GC (CC/CN)	r_AM4 (CN)	r_GC (CN)
Stratospheric intrusions							
April 22-23	58.9/64.1	63.9/67.2	51.3/55.8	5.0/3.1	-7.5/-8.4	0.7	0.9
May 13-14	63.7/61.0	69.1/62.2	55.2/54.9	5.4/1.2	-8.4/-6.1	-0.5	0.8
June 11-13	53.3/55.2	62.4/62.1	48.2/48.5	9.2/6.9	-5.1/-6.7	0.8	0.9
Combined stratospheric and regional pollution influences							
June 14	64.8/56.6	68.1/62.4	56.7/52.9	3.4/5.8	-8.1/-3.7	0.9	0.9
Wildfires							
June 22	66.7/57.4	55.5/58.0	70.5/58.5	-11.2/0.5	3.7/1.1	0.6	0.7
Regional/local pollution events							
June 2	60.7/57.1	59.3/53.8	58.8/55.1	-1.4/-3.4	-1.9/-2.1	0.6	0.9
June 16	67.1/53.8	65.4/55.5	66.7/53.2	-0.5/1.6	3.8/-0.7	0.9	0.9
June 29-30	66.2/57.1	56.2/54.8	62.3/53.6	-10.0/-2.2	-3.9/-3.5	0.7	0.9
Long-range transport of Asian pollution							
May 24	62.9/56.1	62.4/60.3	66.7/54.5	-0.5/4.3	3.8/-1.5	0.7	0.7
Unattributed event							
June 28	66.3/55.9	53.8/52.8	60.3/55.6	-12.5/-3.1	-5.9/-0.3	0.6	0.8

Table S5. Interannual variability of May-June mean MDA8 O_3 from observations and GFDL-AM4 BASE simulations (C96_BASE; Table S3) at 14 Clark County air quality monitoring sites during 2010-2017, along with model-estimated contributions from U.S. background (USB), North American Background (NAB), stratosphere-to-troposphere transport (O_3Strat), long-range transport of Asian pollution (ASIA), and wildfires (FIRE).

May-Jun	**OBS**	**BASE**	**USB**	**NAB**	**O_3Strat**	**ASIA**	**FIRE**
2010	58.2	63.2	52.6	48.9	20.5	4.7	2.3
2011	60.6	65.3	54.1	50.9	22.0	5.7	3.4
2012	64.3	65.7	55.3	51.6	20.4	4.2	2.7
2013	61.2	63.7	53.7	50.7	20.4	4.6	2.5
2014	59.2	61.8	51.5	47.4	18.4	4.3	1.4
2015	59.3	63.9	51.8	46.6	16.5	3.3	1.5
2016	56.4	60.7	48.9	44.3	14.9	3.8	1.8
2017	57.0	61.7	50.9	46.8	17.9	4.2	2.2
Mean±s.d.	59.5±2.5	63.2±1.8	52.3±2.0	48.4±2.6	18.9±2.4	4.4±0.7	2.2±0.7

Table S6. Percentage of site-days with MDA8 O_3 greater than 70 ppbv or 65 ppbv at air quality monitoring sites in Clark County and at CASTNet sites from observations (OBS), GFDL-AM4 (AM4) and GEOS-Chem (GC) simulations during April-June of 2010-2017. See Table S1 for the locations of sites.

	> 70 ppbv			**> 65 ppbv**		
Clark County sites	**OBS**	**AM4**	**GC**	**OBS**	**AM4**	**GC**
2010	4.1%	8.2%	/	15.5%	32.7%	/
2011	9.8%	15.4%	/	23.5%	39.8%	/
2012	15.6%	20.2%	/	31.0%	45.6%	/
2013	9.2%	9.5%	/	24.6%	41.8%	/
2014	5.6%	6.8%	/	14.3%	25.8%	/
2015	4.9%	10.3%	/	16.1%	37.6%	/
2016	1.9%	4.0%	/	8.8%	28.8%	/
2017	2.4%	4.6%	1.3%	10.8%	22.0%	6.1%
Mean±s.d.	6.7%±4.6%	9.9%±5.5%	/	18.1%±7.6%	34.3%±8.3%	/
CASTNet sites	**OBS**	**AM4**	**GC**	**OBS**	**AM4**	**GC**
2010	2.8%	6.5%	/	10.8%	23.0%	/
2011	6.7%	7.7%	/	17.5%	27.2%	/
2012	9.4%	7.7%	/	24.2%	33.4%	/
2013	1.8%	3.5%	/	10.0%	17.0%	/
2014	1.1%	0.7%	/	5.0%	8.4%	/
2015	1.3%	2.2%	/	5.0%	16.4%	/
2016	0.4%	1.3%	/	3.3%	12.6%	/
2017	0.9%	2.0%	0.1%	4.6%	15.5%	1.3%
Mean±s.d.	3.1%±3.2%	4.0%±2.9%	/	10.1%±7.4%	19.2%±8.2%	/

References

Austin, J., and Wilson, R. J.: Ensemble simulations of the decline and recovery of stratospheric ozone, J. Geophys. Res.-Atmos., 111, https://doi.org/10.1029/2005JD006907, 2006.

Austin, J., Horowitz, L. W., Schwarzkopf, M. D., Wilson, R. J., and Levy II, H.: Stratospheric Ozone and Temperature Simulated from the Preindustrial Era to the Present Day, J. Climate, 26, 3528-3543, https://doi.org/10.1175/jcli-d-12-00162.1, 2013.

Donner, L. J., Wyman, B. L., Hemler, R. S., Horowitz, L. W., Ming, Y., Zhao, M., Golaz, J.-C., Ginoux, P., Lin, S.-J., Schwarzkopf, M. D., Austin, J., Alaka, G., Cooke, W. F., Delworth, T. L., Freidenreich, S. M., Gordon, C. T., Griffies, S. M., Held, I. M., Hurlin, W. J., Klein, S. A., Knutson, T. R., Langenhorst, A. R., Lee, H.-C., Lin, Y., Magi, B. I., Malyshev, S. L., Milly, P. C. D., Naik, V., Nath, M. J., Pincus, R., Ploshay, J. J., Ramaswamy, V., Seman, C. J., Shevliakova, E., Sirutis, J. J., Stern, W. F., Stouffer, R. J., Wilson, R. J., Winton, M., Wittenberg, A. T., and Zeng, F.: The Dynamical Core, Physical Parameterizations, and Basic Simulation Characteristics of the Atmospheric Component AM3 of the GFDL Global

Coupled Model CM3, J. Climate, 24, 3484-3519, https://doi.org/10.1175/2011jcli3955.1, 2011.

Horowitz, L. W., Walters, S., Mauzerall, D. L., Emmons, L. K., Rasch, P. J., Granier, C., Tie, X., Lamarque, J.-F., Schultz, M. G., Tyndall, G. S., Orlando, J. J., and Brasseur, G. P.: A global simulation of tropospheric ozone and related tracers: Description and evaluation of MOZART, version 2, J. Geophys. Res.-Atmos., 108, https://doi.org/10.1029/2002JD002853, 2003.

Horowitz, L. W., Fiore, A. M., Milly, G. P., Cohen, R. C., Perring, A., Wooldridge, P. J., Hess, P. G., Emmons, L. K., and Lamarque, J.-F.: Observational constraints on the chemistry of isoprene nitrates over the eastern United States, J. Geophys. Res.-Atmos., 112, https://doi.org/10.1029/2006JD007747, 2007.

Lin, J.-T., and McElroy, M. B.: Impacts of boundary layer mixing on pollutant vertical profiles in the lower troposphere: Implications to satellite remote sensing, Atmos. Environ., 44, 1726-1739, https://doi.org/10.1016/j.atmosenv.2010.02.009, 2010.

Murray, L. T., Jacob, D. J., Logan, J. A., Hudman, R. C., and Koshak, W. J.: Optimized regional and interannual variability of lightning in a global chemical transport model constrained by LIS/OTD satellite data, J. Geophys. Res.-Atmos., 117, https://doi.org/10.1029/2012jd017934, 2012.

Naik, V., Horowitz, L. W., Fiore, A. M., Ginoux, P., Mao, J., Aghedo, A. M., and Levy II, H.: Impact of preindustrial to present-day changes in short-lived pollutant emissions on atmospheric composition and climate forcing, J. Geophys. Res.-Atmos., 118, 8086-8110, https://doi.org/10.1002/jgrd.50608, 2013.

Price, C., and Rind, D.: A simple lightning parameterization for calculating global lightning distributions, J. Geophys. Res.-Atmos., 97, 9919-9933, https://doi.org/10.1029/92JD00719, 1992.